

# Physical adsorption of xenon in open single walled carbon nanotubes: Observation of a quasi-one-dimensional confined Xe phase

A. Kuznetsova and J. T. Yates, Jr.

*Department of Chemistry, Surface Science Center, University of Pittsburgh, Pittsburgh, Pennsylvania 15260*

J. Liu and R. E. Smalley

*Department of Chemistry, Rice University, Houston, Texas 77005*

(Received 8 September 1999; accepted 7 January 2000)

The adsorption of Xe into carbon single walled nanotubes with both closed and open ends has been investigated using temperature programmed desorption and other surface analytical tools. It has been found that opening the ends of the nanotube by chemical cutting increases both the kinetic rate and the saturation capacity of the nanotubes for Xe at 95 K. Further enhancement in Xe adsorption kinetics and capacity are achieved by treating the nanotubes in vacuum at 1073 K where CO, CO<sub>2</sub>, CH<sub>4</sub>, and H<sub>2</sub> are evolved. On this basis it is postulated that surface functionalities such as -COOH block entry ports for adsorption at the nanotube ends and at the defect sites on the walls. The thermal destruction of these functionalities leads to enhanced adsorption. The denser phase of Xe inside the saturated nanotubes desorbs by zero-order kinetics ( $E_d = 26.8 \pm 0.6$  kJ/mol). It is postulated that a quasi-one-dimensional Xe confined phase in equilibrium, with a two-dimensional Xe gas phase on the exterior, provides a phase transition governing the zero-order kinetics desorption process. © 2000 American Institute of Physics. [S0021-9606(00)71313-4]

## I. INTRODUCTION

A theoretical and experimental understanding of carbon nanotubes has developed very rapidly over the last few years. The mechanical and electronic properties of nanotubes are interesting and give promise for useful nanotube applications in nano-engineering<sup>1-4</sup> and as catalyst supports.<sup>5</sup> The unique shape of carbon nanotubes (hollow pipes up to 1  $\mu\text{m}$  length) make nanotubes useful for physical adsorption, and this paper deals with this phenomenon.

Carbon nanotubes produced by the catalytic method are believed to have closed ends, composed of pentagonal and hexagonal carbon rings. The opening of the ends is achieved by cutting the tubes using an acidic and oxidizing solution with sonication.<sup>6</sup> This cutting procedure provides openings in the nanotube for adsorption on the inner surface. The introduction of metals and metal salts inside nanotubes demonstrates the availability of the nanotube interior for interaction with other substances.<sup>3,7-10</sup>

The curvature of the nanotube interior compared to a plane graphitic sheet is expected to cause enhanced adsorption properties for gaseous species, including hydrogen and the rare gases. Theoretical studies predict an increased adsorption capacity and adsorption binding energy of open-ended nanotubes.<sup>11-16</sup>

Theoretical findings about adsorption into nanotubes have been awaiting experimental verification. A few studies of the adsorption of gases have appeared during the last two years. Ultrahigh pressures were used to introduce Ar into the interior of nanotubes.<sup>17</sup> The experiment is complicated by the existence of multiwalls and large amounts of impurities, which can incorporate gas species in regions other than the nanotube interior. The adsorption of hydrogen was studied on nanotube samples of only 0.2% purity.<sup>18</sup> These results

have been extended to a higher purity nanotube sample.<sup>19</sup> The adsorption isotherm of N<sub>2</sub> was measured on nanotubes with a broad distribution of diameters and wall layer thicknesses, including also mesoporous multiwall nanotubes.<sup>20</sup> The saturation adsorption of N<sub>2</sub>, benzene and methanol inside of chemically cut single walled nanotubes (SWNTs) has been shown to exceed that of uncut SWNTs.<sup>21</sup>

In this paper we report the results of Xe adsorption experiments performed on single wall carbon nanotubes. Fullerene pipes (*o*-SWNTs) and fullerene ropes (*c*-SWNT) with open and closed ends, respectively, and with identical mass were studied under ultrahigh vacuum conditions using samples of the nanotubes with high purity. Measurements of the elemental purity of the SWNTs were carried out using Auger electron spectroscopy and x-ray photoelectron spectroscopy. Xe adsorption/desorption measurements were done using temperature programmed desorption (TPD). The measured kinetics of Xe desorption provide new physical insight into the mechanism of Xe transport to and from the interior of the SWNTs as well as evidence for a quasi-1D confined Xe phase inside the open nanotubes.

## II. EXPERIMENT

### A. Carbon nanotube samples

Single walled carbon nanotubes were produced using the technique described previously<sup>6</sup> in which collected material was purified by HNO<sub>3</sub>/H<sub>2</sub>SO<sub>4</sub> treatment. The measured purity of these samples is >90% using TEM and AFM measurement. The nanotube diameter distribution centered near that of (10,10) SWNTs with diameter of 13.6 Å.<sup>22,23</sup> The purified sample of nanotubes were suspended in methanol and deposited onto evaporated Au films on a Ta foil. The

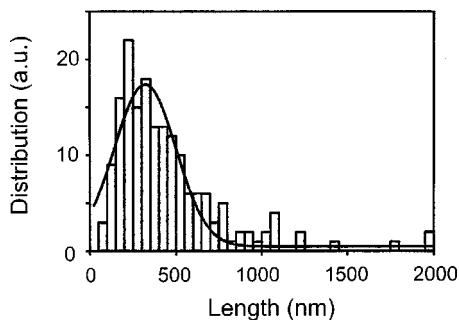


FIG. 1. Length distribution for *o*-SWNT sample. The average length is near 320 nm.

samples are believed to have closed ends as they were produced and are designated as *c*-SWNT samples in this work.

The samples of open-end nanotubes (*o*-SWNTs) were prepared by cutting the purified sample using an  $\text{HNO}_3/\text{H}_2\text{SO}_4$  mixture and sonication followed by treatment in  $\text{H}_2\text{O}_2/\text{H}_2\text{SO}_4$ . The length distribution of *o*-SWNTs as measured from AFM images is shown in Fig. 1. Both samples of open- and closed-end carbon nanotubes were deposited from the methanol suspension in a  $1\text{ cm}^2$  spot onto the Au-covered Ta foil by the drop/dry technique. The nanotubes are held on the Au surface by van der Waals forces. As will be described later, the nanotube samples were heated in ultrahigh vacuum to 623 K or 1073 K prior to Xe adsorption. The mass of the open- and closed-end nanotube samples used was  $46\ \mu\text{g}$ . The Au-plated Ta foils are rigidly and reproducibly fixed between two Ta rods by interlock holders described elsewhere.<sup>24</sup> The cooling of the sample below 95 K was achieved by bubbling  $\text{He}(g)$  through a  $l\text{-N}_2$  column in the manipulator tube which lowers the cryogenic fluid temperature to the  $\text{N}_2$  triple point (63 K).<sup>25</sup> Using this method we achieved a minimum sample temperature of 82 K after Xe adsorption experiments at 95 K, and all temperature programming also started at 82 K. The samples were reproducibly programmed linearly in temperature at a ramp rate of 1.0 K/s using a type *K* thermocouple and Labview software. The accuracy of the temperature is  $\pm 0.2\text{ K}$ . An accurate comparison of Xe adsorption on the nanotube sample and onto an identical clean Au/Ta support foil was made for each adsorption experiment at equivalent Xe exposures. Adsorption by the support is reproducible and does not exceed a few percent of the nanotube adsorption in any of the measurements.

Raman spectra were taken on as prepared and annealed nanotube *o*-SWNT materials using 782 nm diode laser and 514 nm Ar ion laser.

## B. Vacuum techniques

The experiments were done under ultrahigh vacuum conditions with a base pressure in the chamber of  $8 \times 10^{-11}$  Torr. The chamber is equipped with 360 L/s ion pump, a 150 L/s turbo pump and a titanium sublimation pump. As shown in Fig. 2, the TPD measurements were done using an apertured quadrupole mass spectrometer (UTI Instruments/100 C). This permits measurements of the thermal desorption of Xe from the nanotubes while discriminating against possible desorption from the surrounding region of the cooled support

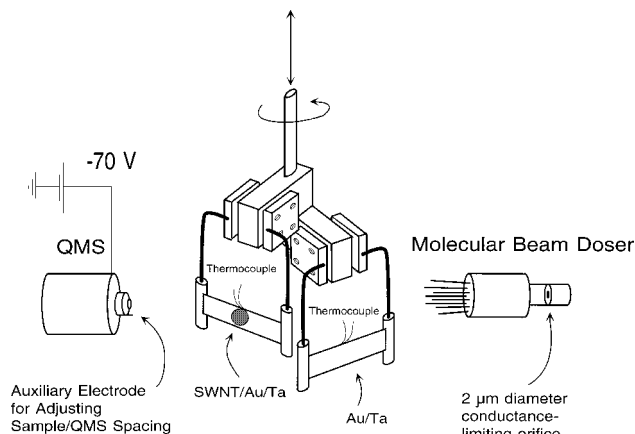


FIG. 2. Experimental apparatus, containing 2-sample manipulator, quadrupole mass spectrometer (QMS), and molecular beam doser.

assembly. The aperture of the QMS is biased to  $-70\text{ V}$  to exclude the possible effect of stray electron emission from the thermionic emitter of the QMS. The mass spectrometer was calibrated against a Bayard–Alpert ionization gauge assuming a gauge sensitivity ratio of Xe and  $\text{N}_2$  of 2.7.<sup>26</sup> It was shown that the QMS response was linear over a wide Xe pressure range. The sensitivity of the mass spectrometer to emission current was carefully measured for currents of 0.5 mA and 2.0 mA, used, respectively, for high and low intensity Xe TPD measurements.

The auxiliary tungsten contacting electrode (shown in Fig. 2) is used as a fiducial point (using the micrometer on the sample manipulator) to accurately and reproducibly locate the sample 1 mm away from the 3.0 mm diameter aperture for controlled measurement of the TPD spectra.

The xenon gas (99.995% purity, Matheson) was introduced into the system from a pyrex flask through a collimated and calibrated molecular beam doser, shown in Fig. 2. It provides a known uniform flux of Xe molecules creating a local high pressure (compared to the background pressure) of adsorbate at the sample surface.<sup>27</sup> The doser was calibrated with Xe gas and was shown to give an absolute Xe delivery rate of  $7.2 \pm 1.2 \times 10^{13}$  molecules Torr<sup>-1</sup> s<sup>-1</sup>. From the calculation of the fractional interception of the gas beam by the sample estimated from the doser/sample geometry,<sup>27</sup> the incident Xe flux is  $5.3 \times 10^{13}$  molecules cm<sup>2</sup> s<sup>-1</sup> at a backing pressure of 1.8 Torr Xe. The exposure of the nanotube sample to the xenon flux was performed at 95 K. For Xe exposures above  $2 \times 10^{18}$  molecules/cm<sup>2</sup>, adsorption was carried out by filling the vacuum chamber to Xe pressures from  $3.7 \times 10^{-6}$  Torr to  $3.7 \times 10^{-4}$  Torr using the ionization gauge for measurements. Prior to the TPD measurement, Xe was pumped away from the chamber to a pressure below  $\sim 4 \times 10^{-9}$  Torr.

## C. Surface spectroscopy

A hemispherical Leybold–Heraeus EA-10 electron analyzer oriented at  $45^\circ$  to the sample was used for XPS studies of the carbon nanotube samples. The calibration of the XPS energy scale was done using the Au  $4f_{7/2}$  transition. The Al  $K_\alpha$  line of 1486.6 eV energy was used for XPS measurements. Based on this calibration the binding energy accuracy in multiple measurements was estimated to be  $\pm 1.0\text{ eV}$ .

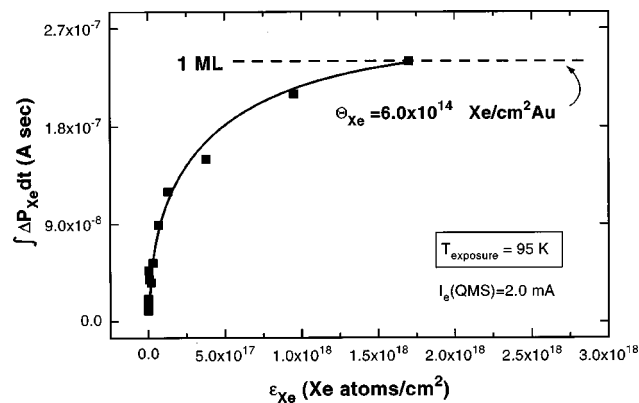


FIG. 3. Adsorption of Xe on polycrystalline Au support surface to saturation coverage of  $6.0 \times 10^{14}$  Xe/cm<sup>2</sup>. This measurement is used for calibration of the Xe coverage on *c*-SWNT and *o*-SWNT samples.

A Perkin Elmer Auger spectrometer (Model 11-010-cylindrical mirror analyzer) was used for the characterization of SWNT samples by Auger electron spectroscopy. The primary beam energy used was 3 keV, and an emission current of 0.2  $\mu$ A was employed.

#### D. Estimates of absolute Xe coverages

The coverage of Xe on the nanotube samples was determined using the desorption peak area from the Au support surface as a standard. The literature shows that the surface of various metals saturates with a monolayer coverage of xenon under the same conditions as in our experiment. Thus W(111) and Pt(111) surfaces can accommodate 1 ML of xenon atoms at 95 K.<sup>28-30</sup>

Figure 3 shows the rise in Xe coverage on the clean Au with increasing exposure to Xe at 95 K, as judged from the integrated Xe TPD peak. The saturation coverage reached is assumed to correspond to a close-packed Xe overlayer with a surface coverage of  $6.0 \times 10^{14}$  Xe/cm<sup>2</sup>.<sup>30</sup> This value is employed as a calibration standard for Xe desorption studies from the various nanotube samples. In addition, in all measurements, the Xe coverage measured from the nanotube samples has been corrected for the small Xe desorption contribution from the clean Au surface using these data.

We therefore report the absolute coverage of Xe on the nanotubes in terms of the atomic ratio of Xe to C as  $N_{Xe}/N_C$ . In addition the initial sticking coefficient for Xe is reported as an absolute rate of Xe adsorption per Xe collision on the nanotube exterior.

### III. EXPERIMENTAL RESULTS

#### A. Thermal desorption spectra of Xe from single walled nanotubes prepared at 623 K

Figure 4 shows the series of temperature programmed desorption spectra of xenon after exposure to different fluences of xenon. This experimental series was performed after the activation of nanotubes at 623 K.

A series of TPD spectra obtained for closed single walled nanotubes is shown on the left-hand side of Fig. 4 stacked together for increasing Xe exposure. A small single

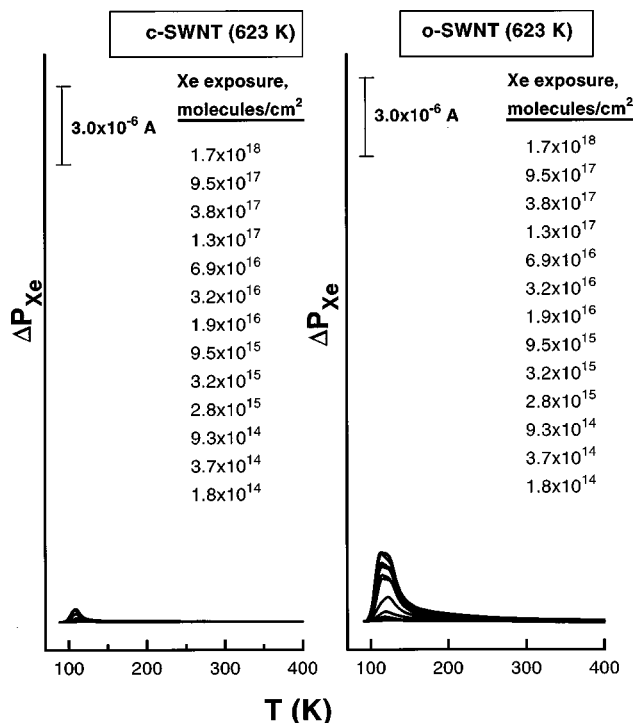


FIG. 4. Comparison of Xe temperature programmed desorption on *c*-SWNT and *o*-SWNT samples after activation in vacuum at 623 K, for various Xe exposures.

desorption peak is observed here. For the open single walled nanotubes (shown in the right portion of Fig. 4) at least two peaks are contained in the desorption feature and they largely overlap with each other.

The integrated areas of the Xe desorption peaks are shown as a function of Xe exposure in Fig. 5. The ordinate of Fig. 5, expressed as the ratio  $N_{Xe}/N_C$ , is calculated on the basis of the integrated Xe TPD signal from the known mass of nanotubes deposited on the 1 cm<sup>2</sup> spot.

As shown in Fig. 5, the Xe uptake of the open-end carbon nanotube sample is much higher than the uptake for the closed-end nanotubes, prepared at 623 K. The initial sticking coefficient measured as the slope of the coverage-exposure

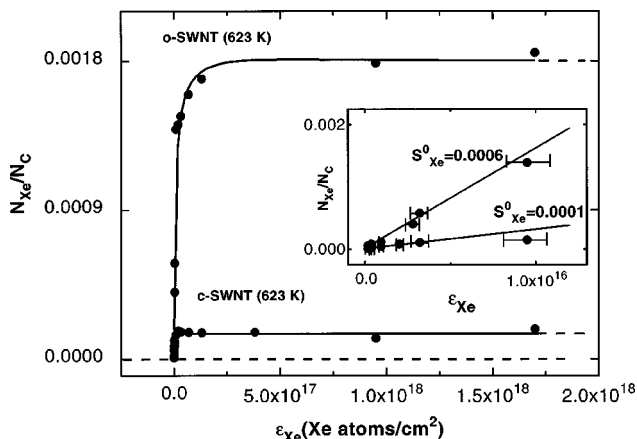


FIG. 5. Adsorption of xenon on *c*-SWNT and *o*-SWNT samples after activation at 623 K. The initial sticking coefficient,  $S_{Xe}^0$ , is determined from the slope of the initial portion of the curve (shown in the inset).

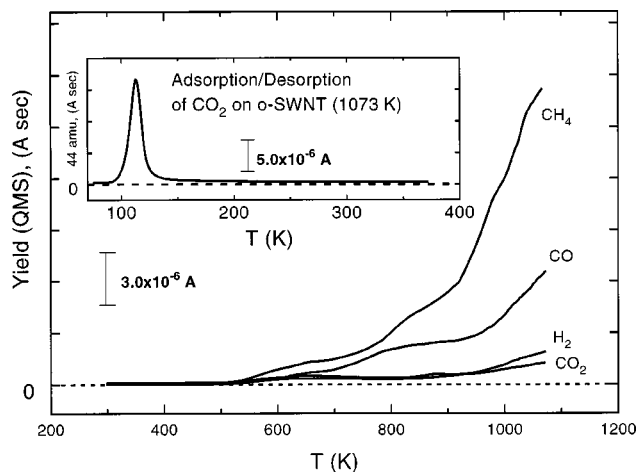


FIG. 6. Initial activation of *o*-SWNT sample. The *c*-SWNT samples show similar gas evolution spectra. The inset shows the desorption spectrum for CO<sub>2</sub> which has been adsorbed purposely on the *o*-SWNT (1073 K) sample.

plot is found to be 0.0001 for the closed-end sample and 0.0006 for the open-end sample. In this sticking coefficient measurement we approximate a surface area of  $2.6 \text{ \AA}^2/\text{C}$  atom which is the area per carbon atom on a flat graphite sheet. Figure 5 shows that the Xe uptake at saturation for the open-end nanotubes prepared at 623 K is 12 times higher than for the closed-end nanotubes.

## B. High temperature activation of nanotubes

The gas evolution observed during the thermal activation of the nanotube samples with open ends is shown in Fig. 6. We observed the evolution of CO, CO<sub>2</sub>, H<sub>2</sub>, and CH<sub>4</sub> gas during annealing at temperatures up to 1073 K. The onset temperature of the gas evolution is around 500 K. The gas evolution from the *c*-SWNT sample was very similar in magnitude and in desorption peak distribution to that shown in Fig. 6. This observation demonstrates that the level of functionalization of SWNTs as measured by gas evolution on heating is not a means to discriminate *o*-SWNTs from *c*-SWNTs as suggested previously.<sup>6</sup>

The origin of the CO<sub>2</sub> desorption feature was studied by a control experiment involving CO<sub>2</sub> physisorption from the gas phase. After the exposure of the 1073 K annealed open-ended nanotube sample to CO<sub>2</sub> a TPD spectrum was taken. The desorption peak of CO<sub>2</sub> in this case occurs at 112 K (shown in the inset to Fig. 6) as compared to the 500 K onset temperature for CO<sub>2</sub> evolution during thermal activation. Thus, the CO<sub>2</sub> observed above  $\sim 600$  K from both *o*-SWNTs and *c*-SWNTs must be due to a chemical decomposition process in the nanotube material. Similarly, H<sub>2</sub>, CO, and CH<sub>4</sub> must also originate from a chemical decomposition process in the nanotube material.

## C. Xe adsorption on activated (1073 K) nanotubes

Another series of Xe TPD spectra was taken after *o*-SWNT and *c*-SWNT samples were annealed at 1073 K. The uptake of xenon on both *o*-SWNTs and *c*-SWNTs increased, but to a larger extent for the *o*-SWNTs. The inte-

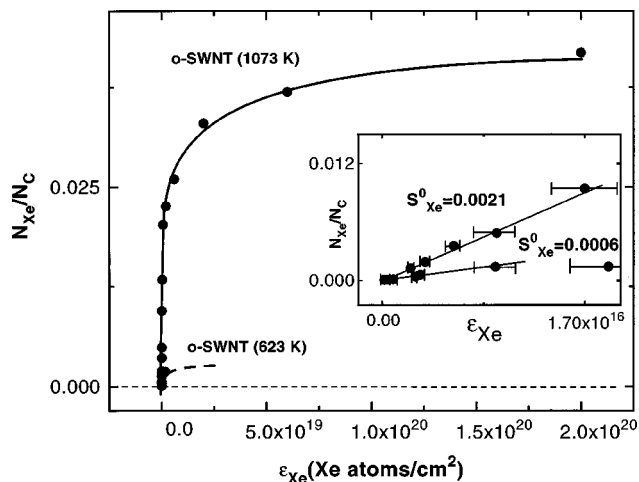


FIG. 7. Adsorption of xenon on *o*-SWNT after activation at 623 and 1073 K. The initial sticking coefficient,  $S_{\text{Xe}}^0$ , is determined from the slope of the initial portion of the curve (shown in the inset).

grated area of the Xe desorption, representing the coverage of Xe achieved at these exposures for *o*-SWNT, is shown in Fig. 7.

An approximately 23-fold increase in the saturation capacity of Xe on the *o*-SWNTs is observed, comparing the 623 K activation to the 1073 K activation. In addition, activation at 1073 K causes the initial sticking coefficient of Xe to increase from 0.0006 (Fig. 5) to 0.0021 (Fig. 7).

Figure 8 displays the stacked Xe TPD spectra for a wide range of Xe exposure on *c*-SWNTs (1073 K) and *o*-SWNTs (1073 K) which form the basis for Fig. 7. For the *c*-SWNTs, two weak Xe desorption features are observed at about 105 K and 120 K at the highest Xe exposure. For the *o*-SWNTs,

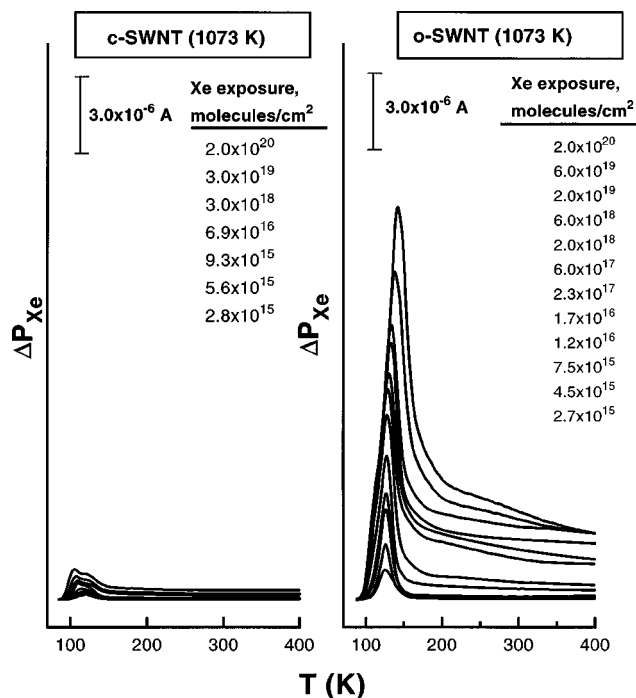


FIG. 8. Comparison of Xe temperature programmed desorption on *c*-SWNT and *o*-SWNT sample after activation at 1073 K.

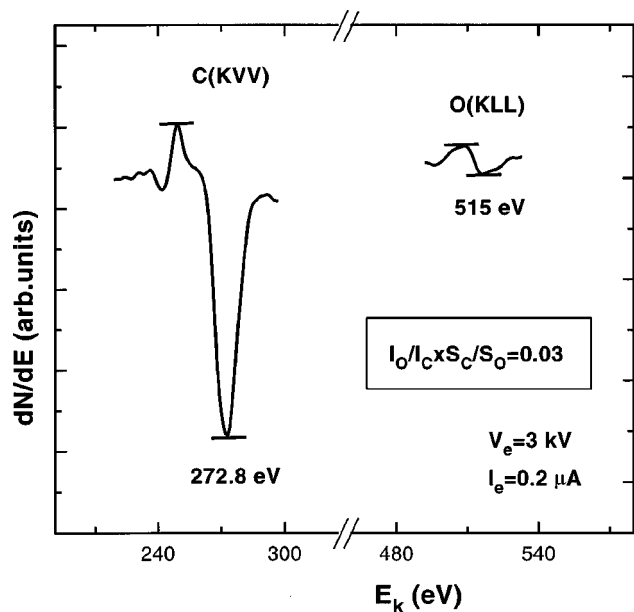


FIG. 9. Auger spectrum of *o*-SWNT (1073 K) sample. A similar spectrum is observed for the *c*-SWNT (1073 K) sample. An atomic fraction of 0.03 O is observed in the depth of Auger sampling.

the 120 K feature dominates in the TPD spectra and this feature develops and shifts to higher temperature as the Xe coverage increases. The coalescence of the leading edge of the Xe TPD spectra beginning at a Xe exposure of  $6 \times 10^{17}$  Xe/cm<sup>2</sup> is evident. In addition, a pronounced desorption tail above about 200 K is observed for the higher Xe exposures.

#### D. Auger spectroscopic and XPS characterization of nanotubes

The Auger spectrum of the nanotube samples after 1073 K activation is shown in Fig. 9. The C(KVV) transition is observed at 272.8 eV. The C(KVV) Auger line shape is very similar to that of graphite.<sup>31</sup>

The O(KLL) transition at 515 eV was also observed. This is associated with remaining oxygen functionalities on the (*o*- or *c*-) SWNTs and no differences were observed between *o*- and *c*-SWNT samples. The atomic fraction of oxygen in the depth of Auger sampling is estimated to be 0.03 from the intensity comparison for the O(KLL) and C(KVV) transition using the formula  $C_O/C_C = I_O/I_C \times S_C/S_O$ ;  $C$ =concentration of oxygen or carbon;  $I$ =intensity of Auger peak; and  $S$ =sensitivity for oxygen or carbon from Ref. 31. Within the detection limits of Auger spectroscopy no other elements were observed. The contribution to the O and C intensities from the Au substrate were negligible, as determined in control experiments on the Au blank.

Figure 10 shows the C(1s) transition for the *o*- or *c*-SWNT (1073 K) samples. A similar spectrum was observed for the *c*-SWNT (1073 K) sample. This C(1s) binding energy is about 1.3 eV lower than the binding energy of graphite, which is consistent with the measurements of others, where C(1s) binding energies from 0.3 eV to 0.5 eV lower than that for graphite were observed for nanotubes.<sup>32,33</sup> The shape of the C(1s) peak is similar to the shape of the

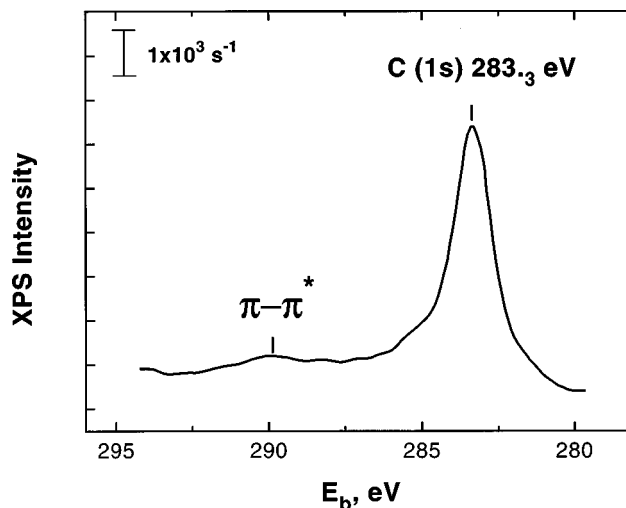


FIG. 10. XPS spectrum of the *o*-SWNT (1073 K) sample. A similar spectrum is observed for the *c*-SWNT (1073 K) sample.

C(1s) peak of graphite. Small features on the high binding energy side at 290 eV are, on graphite and on aromatic polymers, related to the  $\pi-\pi^*$  transitions, accompanying the C(1s) excitation.<sup>34,35</sup>

Figure 11 shows the Raman spectral region of unheated *o*-SWNTs and annealed *o*-SWNTs (1073 K). The similarity of the spectra is a strong indicator that the tube structure of the *o*-SWNT is not influenced significantly in this heating process.

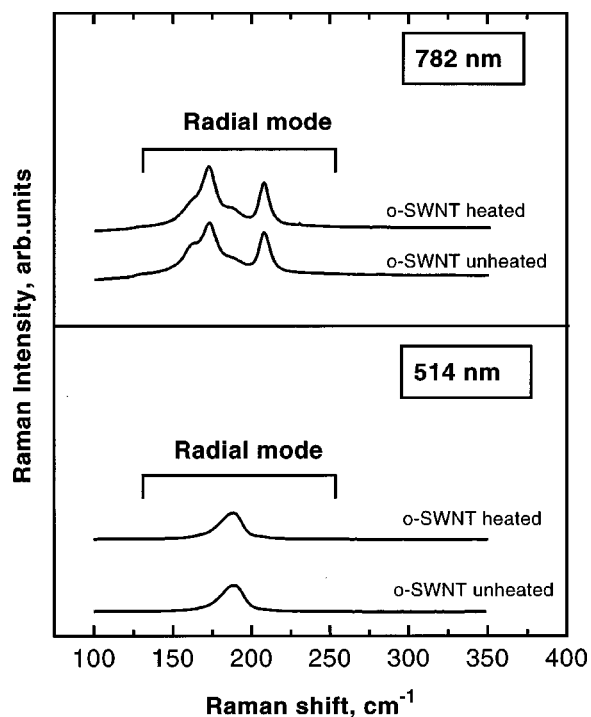


FIG. 11. Raman spectral comparison of unheated *o*-SWNTs and heated *o*-SWNTs. The similarity of the two spectra indicates that the tube structure of the SWNTs is not perturbed by annealing in ultrahigh vacuum.

## IV. DISCUSSION

### A. Preparation of closed-end and open-end single wall nanotubes (*o*-SWNTs and *c*-SWNTs)

As produced nanotubes are believed to be composed of long bundles of intertwisted tubes, which have closed ends. The closing of the ends with a cap is the cause of the growth termination. The length of these bundles can be a few micrometers.

To open nanotubes a number of techniques could be employed.<sup>1-3</sup> One tube opening method, used for this work, involves treatment in oxidizing HNO<sub>3</sub>/H<sub>2</sub>SO<sub>4</sub> solution and sonication followed by H<sub>2</sub>O<sub>2</sub>/H<sub>2</sub>SO<sub>4</sub>. As a result the closed ends of nanotubes are etched away. The nanotube opening process is also accompanied by a tube cutting process, resulting in a rather sharp distribution of tube lengths, as shown in Fig. 1.

Our Xe adsorption results provide the first physical evidence that cutting the nanotubes causes enhanced internal adsorption to be possible.

Together with cutting, the acidic treatment may also cause the oxidation of regions the nanotube surface. A number of studies on the oxidation of graphite<sup>4,36</sup> showed that an oxidizing agent like nitric acid can attack a graphite surface mainly by creating oxygenated groups, such as C=O, O=C-O, C-OH, and C-O-C. These groups are formed preferentially at the edges of large defects—steps or deep holes present on the graphite surface, as observed by STM. We believe that similar functional groups are present on the nanotubes employed here. Based on the observation of CH<sub>4</sub>, CO, H<sub>2</sub>, and CO<sub>2</sub> evolution above 600 K for both uncut and cut nanotube samples, these functionalities must be present in both samples at approximately the same fractional composition. This is reasonable, since the fraction of tube end carbon atoms in a 320 nm SWNT is of order 10<sup>-3</sup>.

### B. Thermal treatment of nanotubes in vacuum

The activation of nanotubes by heating in vacuum from 623 K to 1073 K has been shown to enhance Xe adsorption at 95 K. In the case of the *c*-SWNT sample, the Xe capacity increases by about a factor of 10: for *o*-SWNT sample, heating to 1073 K increases the Xe adsorption capacity by a factor of about 23.

It is likely that C=O, O=C-O, and C-OH groups, and possibly other oxidized groups are formed by oxidation at the tube ends and at defect sites on the tube walls. Bound oxygen and hydrogen in the functional groups stabilize the carbon dangling bonds at these sites. The bulky surface groups are present at the tube ends. For *o*-SWNT activation temperature above ~580–600 K, these functional groups begin to decompose, yielding CO<sub>2</sub>, CO, CH<sub>4</sub>, and H<sub>2</sub>. This process of chemical removal of the blocking functionalities by thermal decomposition opens entry ports into the nanotube interior causing two effects:

- (1) Enhanced Xe saturation capacity.
- (2) Enhanced Xe adsorption kinetics rate (sticking probability).

For *c*-SWNTs which have not been chemically cut, heating from 623 K to 1073 K in vacuum also opens some entry ports into the nanotubes, but the Xe capacity and Xe sticking coefficient on such samples is always far below that found on *o*-SWNTs.

### C. Comparison of *c*-SWNT (623 K) and *o*-SWNT (623 K) using Xe adsorption

Figures 4 and 5 show the comparison of the Xe desorption kinetics, the Xe sticking coefficient, and the Xe saturation coverage for *c*-SWNTs and *o*-SWNTs which have been activated in vacuum at 623 K. Figure 4 shows that differences in the Xe desorption kinetics exist for the *c*-SWNT and *o*-SWNT samples. A desorption process near 120 K is observed on the *o*-SWNT which is not present on the *c*-SWNT sample. Figure 5 shows that the initial sticking coefficient,  $S_{Xe}^0$  increases by a factor of 6 for *o*-SWNTs compared to *c*-SWNTs, both of which have been activated at 623 K. The saturation capacity of Xe is also increased by a factor of 12 from  $N_{Xe}/N_C = 0.00015$  to  $N_{Xe}/N_C = 0.0018$  comparing the *c*-SWNTs (623 K) to the *o*-SWNTs (623 K).

The enhanced rate of Xe adsorption and of the Xe saturation coverage for *o*-SWNTs (623 K) reflect the increased availability of entry ports to the interior of the SWNTs which have been cut by the acidic cutting process with sonication. This comparison involves *o*-SWNTs which possess a significant number of entry ports which contain oxygenated functionalities blocking or retarding Xe entry to the nanotube interior. As will be discussed below, further opening of these entry ports can be achieved by heating to 1073 K.

### D. Comparison of *o*-SWNT (623 K) and *o*-SWNT (1073 K) using Xe adsorption

The effect of the opening of the functionalized entry ports by chemical decomposition of the blocking groups is illustrated by experiments on *o*-SWNTs. After 623 K activation of *o*-SWNTs, only slight decomposition of the oxygenated groups has occurred (see Fig. 6). Upon heating to 1073 K, a significant loss of these blocking groups has occurred judging from the gas evolution measured in Fig. 6. The decomposition of the blocking groups results in an enhancement of the Xe sticking coefficient from  $S_{Xe}^0 = 0.0006$  to  $S_{Xe}^0 = 0.0021$ , and an increase in the saturation capacity from  $N_{Xe}/N_C = 0.0018$  to  $N_{Xe}/N_C = 0.042$ , as shown in Fig. 7.

## E. Summary—effect of opening entry ports on Xe adsorption in nanotubes

### 1. Adsorption control

These experiments have demonstrated two effects controlling adsorption inside of single walled carbon nanotubes. First, it has been shown kinetically, and by quantitative measurements of the Xe saturation coverage, that the chemical cutting of *c*-SWNTs results in an enhanced kinetic rate of Xe capture at 95 K and also in an enhanced Xe saturation coverage. Second, we have demonstrated that HNO<sub>3</sub>/H<sub>2</sub>SO<sub>4</sub> treatment of the nanotubes leaves functional groups containing carbon, oxygen, and hydrogen. These groups block the entry ports to the nanotube interior to some degree, retarding

Xe adsorption. Decomposition of these groups at 1073 K in vacuum leads to further enhancement in the rate of Xe adsorption and increased Xe saturation capacity as the entry ports are opened.

The full dynamic range of the role of entry port formation is large. For *c*-SWNTs prepared at 623 K the saturation Xe coverage is  $N_{\text{Xe}}/N_{\text{C}}=0.00015$ . For *o*-SWNTs, prepared at 1073 K, the Xe saturation coverage is  $N_{\text{Xe}}/N_{\text{C}}=0.0420$ , a factor of 280 increase. Similarly, the initial rate of Xe adsorption increases by a factor of about 21 in comparing the two cases.

## 2. Saturation capacity of Xe in *o*-SWNT (1073 K)

An *unreachable* geometrical upper limit for the saturation coverage of Xe inside of an *o*-SWNT may be estimated from the relative number of C atoms/ $\text{\AA}^2$  in a flat graphene sheet ( $0.38 \text{ C}/\text{\AA}^2$ ) and the number of Xe atoms in a flat close-packed hexagonal monolayer of Xe ( $0.06 \text{ Xe}/\text{\AA}^2$ ). For this flat geometry,  $N_{\text{Xe}}/N_{\text{C}}=0.16 \text{ Xe}/\text{C}$ . Our measurement at saturation yields  $N_{\text{Xe}}/N_{\text{C}}=0.042 \text{ Xe}/\text{C}$  at 95 K in the *o*-SWNT (1073 K). Thus the saturation density of Xe inside the *o*-SWNT is quite high. For comparison, a single chain of Xe atoms, packed at the  $4.4 \text{ \AA}/\text{Xe}$  atom spacing (found in a flat Xe monolayer) inside a  $13.6 \text{ \AA}$  diameter SWNT corresponds to  $N_{\text{Xe}}/N_{\text{C}}=0.014 \text{ Xe}/\text{C}$ .

## F. Phase behavior for Xe-*o*-SWNT (1073 K)

### 1. Detection of quasi-1D confined Xe phase inside the *o*-SWNTs

Unusual desorption kinetic behavior is observed at Xe exposures above  $6 \times 10^{17} \text{ Xe}/\text{cm}^2$  ( $N_{\text{Xe}}/N_{\text{C}} \geq 0.020$ ), as shown in Fig. 8. A distinct coalescence of the leading edges of the multiple desorption traces is observed. This coalescence is indicative of zero-order desorption kinetics, where the rate of desorption is independent of coverage. Zero-order desorption kinetics are often observed from surfaces. For many cases of zero-order desorption kinetics, a phase transition is occurring during desorption. For example, in the case of inert gas adsorption on highly perfect metal single crystals, zero-order desorption kinetics indicate the presence of a 2D ordered layer in equilibrium with a 2D gas, which desorbs.<sup>37</sup> As desorption occurs from the transient 2D gas species, this species is resupplied by a phase transition, which consumes the 2D ordered phase and leads to zero-order kinetics.

The phase behavior of Xe adsorbed on single walled nanotubes should be closely related to the well studied phase equilibria for Xe on graphite. Theoretical estimates of the adsorption potential of Xe on the outer surface of a single walled nanotubes and on a single layer flat graphene surface are very similar, differing only by 2.3 kJ/mol with the Xe being 20% less strongly bound on the outer SWNT surface.<sup>15</sup> The phase diagram of Xe on graphite has been measured by several groups,<sup>38,39</sup> and on the basis of Xe behavior on graphite in the region of temperature and Xe pressure employed in this work, only the 2D Xe gas phase will be stable on the outer surface of *o*-SWNTs (1073 K).

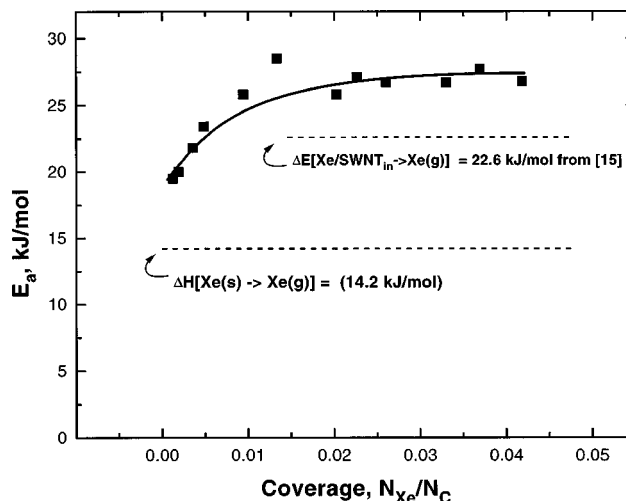


FIG. 12. Activation energy of Xe desorption from *o*-SWNT (1073 K) as measured in the leading edge of the TPD spectrum. The fractional depletion in the leading edge region which was analyzed is  $<3\%$ .

The ratio of Xe coverage on the inside and outside surface of the SWNTs may be estimated using gas-surface virial coefficients,<sup>15,40</sup> which represent the adsorbate interaction over all accessible configurations. Under the conditions in this experiment, the ratio of Xe coverages on the inside compared to the outside of a nanotube is  $\geq 10^6$  at 95 K based on the calculated adsorption energy on the wall exterior of 8.7 kJ/mol.<sup>15</sup> Thus in order to achieve the measured coverages observed here ( $N_{\text{Xe}}/N_{\text{C}}=0.042$ ) another Xe phase which is much more dense than the 2D phase is necessary. This second Xe phase, in equilibrium with the 2D Xe gas phase on the outer wall surface, is responsible for the observation of zero-order kinetics.

These results suggest that a quasi-one-dimensional confined Xe phase is established inside the *o*-SWNT during adsorption, and that this phase desorbs via an equilibrium involving the 2D gas phase on the outer SWNT surface. The 1D Xe phase inside nanotubes is expected on theoretical grounds.<sup>15</sup> One criterion for its existence is that the diameter of the nanotube be two times the diameter of the molecule,<sup>41</sup> which is approximately fulfilled in this work. Recently a 1D He phase has been detected in the interstitial regions which exist between closed SWNTs in bundles.<sup>42</sup> Such interstitial regions cannot be responsible for the 1D phase of Xe postulated here, since the small interstitial site dimensions will not permit Xe atoms to enter these regions.

### 2. Desorption energy for 1D confined Xe phase inside SWNTs (1073 K)

A leading edge analysis<sup>43</sup> of the kinetics of Xe desorption has been performed using the data shown in Fig. 8 for the *o*-SWNTs (1073 K). The coverage dependence of the activation energy for Xe desorption increases up to a Xe coverage of  $N_{\text{Xe}}/N_{\text{C}}=0.020$ , and then becomes constant at a value of  $26.8 \pm 0.6 \text{ kJ/mol}$ , as shown in Fig. 12. The theoretical binding energy of Xe in a  $10 \text{ \AA}$  diameter SWNT has been estimated to be 22.6 kJ/mol,<sup>15</sup> in good agreement with our measurements. The measured activation energy for de-

sorption from the 1D confined Xe phase, in rapid equilibrium with the 2D Xe gas phase on the outer surface, will be equal to or larger than the binding energy of Xe within the nanotubes, depending on whether an activation barrier for adsorption exists. The involvement of the transient 2D Xe gas phase will not affect the desorption activation energy measured for the 1D confined Xe phase.

### 3. Equilibrium for Xe on inner and outer surfaces of SWNTs (1073 K)

The equilibrium between the 2D gas phase on the outer nanotube surface and the 1D confined Xe phase inside the nanotubes is achieved by rapid diffusion through the ends of the *o*-SWNTs and possibly through defect sites on the nanotube walls. Thus the 1D Xe phase is not observed to be kinetically coupled to the 2D gas except for the *o*-SWNTs which have been chemically produced by oxidative cutting and subsequent thermal processing at 1073 K to produce the maximum number of entry ports in the tube ends and possibly in the walls. It is reasonable to postulate on the basis of microscopic reversibility that Xe adsorption into the *o*-SWNT interior also occurs via the 2D gas phase on the nanotube exterior.

## V. SUMMARY OF RESULTS

The following results have been obtained in our study of Xe adsorption on *c*-SWNTs and *o*-SWNTs:

- (1) The Xe adsorption capacity and sticking coefficient on SWNTs is strongly dependent on the preparation conditions. Open SWNTs prepared by H<sub>2</sub>O<sub>2</sub>/H<sub>2</sub>SO<sub>4</sub> treatment exhibit an enhanced Xe adsorption rate and Xe capacity compared to *c*-SWNTs.
- (2) Heating *o*-SWNTs to 1073 K in vacuum evolves CO<sub>2</sub>, CO, CH<sub>4</sub>, and H<sub>2</sub> which originate from surface functionalities present on the nanotube ends and at defect sites on the nanotube surface.
- (3) The destruction of the surface functionalities causes a strong enhancement of the Xe sticking coefficient and the Xe saturation capacity of the *o*-SWNTs as blocking of entry ports by these surface groups is diminished.
- (4) The sticking coefficient of Xe at 95 K is only 0.0021 Xe atoms/C atom in *o*-SWNTs (1073 K), indicating that Xe entry into the nanotube interior is relatively inefficient even for nanotubes possessing the highest number of open entry ports.
- (5) The observed saturation capacity for Xe in *o*-SWNTs (1073 K) is  $N_{\text{Xe}}/N_{\text{C}}=0.042$  corresponding to a high level of filling of the nanotubes with Xe at 95 K.
- (6) In the high coverage range, Xe desorption from *o*-SWNTs (1073 K) exhibits zero-order kinetics, indicative of the involvement of a phase transition during desorption. The activation energy for Xe adsorption in this coverage range is  $26.8 \pm 0.6$  kJ/mol in good agreement with theoretical estimates.
- (7) It is postulated that during desorption, a quasi-1D confined Xe phase inside the *o*-SWNTs (1073 K) is in equilibrium with a 2D gas phase on the outer surface of the

*o*-SWNTs, and that this phase transition is responsible for the observed zero-order desorption kinetics.

- (8) By microscopic reversibility, the adsorption of Xe into the interior of *o*-SWNTs will occur via the 2D gas phase on the nanotube exterior.

## ACKNOWLEDGMENTS

We acknowledge with thanks the support of this work by the Army Research Office. We also thank Professor Milton Cole for incisive help.

- <sup>1</sup> *Fullerenes and Structures*, edited by A. Hirsch, Vol. 199, p. 189 (1999).
- <sup>2</sup> *Carbon Nanotubes: Preparation and Properties*, edited by T. W. Ebbesen (CRC, Boca Raton, 1997).
- <sup>3</sup> M. S. Dresselhaus, G. Dresselhaus, and P. C. Eklund, *Science of Fullerenes and Carbon Nanotubes* (Academic, San Diego, CA, 1996).
- <sup>4</sup> *Novel Forms of Carbon*, edited by C. L. Renschler, D. M. Cox, J. J. Pouch, and Y. Achida (Materials Research Society, Pittsburgh, PA, 1994).
- <sup>5</sup> B. Coq, J. M. Planeix, and V. Brotons, *Appl. Catal., A* **173**, 175 (1998).
- <sup>6</sup> J. Liu *et al.*, *Science* **280**, 1253 (1998).
- <sup>7</sup> D. Ugarte, T. Stöckli, J. M. Bonard, A. Châtelain, and W. A. de Heer, *Appl. Phys. A: Mater. Sci. Process.* **67**, 101 (1998).
- <sup>8</sup> S. C. Tsang, Y. K. Chen, P. J. F. Harris, and M. L. H. Green, *Nature (London)* **372**, 159 (1994).
- <sup>9</sup> J. Sloan, J. Cook, J. R. Heesom, M. L. H. Green, and J. L. Hutchison, *J. Cryst. Growth* **173**, 81 (1997).
- <sup>10</sup> A. Chu *et al.*, *J. Mater. Chem.* **8**, 2752 (1996).
- <sup>11</sup> M. W. Maddox and K. E. Gubbins, *Langmuir* **11**, 3988 (1995).
- <sup>12</sup> M. R. Pederson and J. Q. Broughton, *Phys. Rev. Lett.* **69**, 2689 (1992).
- <sup>13</sup> M. W. Maddox and K. E. Gubbins, *J. Chem. Phys.* **107**, 9659 (1997).
- <sup>14</sup> G. Stan and M. W. Cole, *J. Low Temp. Phys.* **110**, 539 (1998).
- <sup>15</sup> G. Stan and M. W. Cole, *Surf. Sci.* **395**, 280 (1998).
- <sup>16</sup> Q. Wang and J. K. Johnson, *J. Chem. Phys.* **110**, 577 (1999).
- <sup>17</sup> G. E. Gadd *et al.*, *Science* **277**, 933 (1997).
- <sup>18</sup> A. C. Dillon *et al.*, *Nature (London)* **386**, 377 (1997).
- <sup>19</sup> Y. Ye *et al.*, *Appl. Phys. Lett.* **74**, 2307 (1999).
- <sup>20</sup> S. Inoue, N. Ichikuni, T. Suzuki, T. Uematsu, and K. Kaneko, *Langmuir* **102**, 46 (1998).
- <sup>21</sup> M. Eswaramoorthy, R. Sen, and C. N. R. Rao, *Chem. Phys. Lett.* **304**, 207 (1999).
- <sup>22</sup> J. W. G. Wildöer, L. C. Venema, A. G. Rinzler, R. E. Smalley, and C. Dekker, *Nature (London)* **391**, 59 (1998).
- <sup>23</sup> T. W. Odum, J. L. Huang, P. Kim, and C. M. Lieber, *Nature (London)* **391**, 62 (1998).
- <sup>24</sup> J. T. Yates, Jr., in *Experimental Innovations in Surface Science* (Springer, New York, 1998).
- <sup>25</sup> J. Xu, H. J. Jänsch, and J. T. Yates, Jr., *J. Vac. Sci. Technol. A* **11**, 726 (1993).
- <sup>26</sup> NASA Technical Note TND-5285, National Aeronautics and Space Administration, Washington, DC, 1969.
- <sup>27</sup> A. Winkler and J. T. Yates, Jr., *J. Vac. Sci. Technol. A* **6**, 2929 (1988).
- <sup>28</sup> J. T. Yates, Jr. and N. E. Erickson, *Surf. Sci.* **44**, 489 (1974).
- <sup>29</sup> W. Widdra *et al.*, *Phys. Rev. B* **57**, 4111 (1998).
- <sup>30</sup> M. J. Dresser, T. E. Madey, and J. T. Yates, Jr., *Surf. Sci.* **42**, 533 (1974).
- <sup>31</sup> L. E. Davis, N. C. MacDonald, P. W. Palmberg, G. E. Riach, and R. E. Webber, *Handbook of Auger Electron Spectroscopy*, 2nd ed. (Perkin-Elmer, Physical Electronics Division, Eden Prairie, MN, 1976).
- <sup>32</sup> P. Chen, H. B. Zhang, G. D. Lin, and K. R. Tsai, *Chem. J. Chin. Univ.* **19**, 765 (1998).
- <sup>33</sup> P. Chen, X. Wu, X. Sun, J. Lin, W. Ji, and K. L. Tan, *Phys. Rev. Lett.* **82**, 2548 (1999).
- <sup>34</sup> D. Briggs, in *Practical Surface Analysis*, edited by D. Briggs and M. P. Seah (Wiley, Chichester, 1983), Chap. 9.
- <sup>35</sup> A. Dilks, in *Electron Spectroscopy—Theory, Techniques, and Applications*, edited by C. R. Brundle and A. D. Baker (Academic, London, 1981), Vol. 4.
- <sup>36</sup> M. Phaner-Goutorbe, A. Sartre, and L. Porte, *Microsc. Microanal. Microstruct.* **5**, 283 (1994).
- <sup>37</sup> W. Widdra, P. Trischberger, W. Frieß, and D. Menzel, *Phys. Rev. B* **57**, 4111 (1998).

<sup>38</sup>M. Bienfait and J. A. Venables, *Surf. Sci.* **64**, 425 (1977).

<sup>39</sup>P. A. Heiney, P. W. Stephens, R. J. Birgeneau, P. M. Horn, and D. E. Monston, *Phys. Rev. B* **28**, 6416 (1983).

<sup>40</sup>The Xe-C interaction potential was taken as a Lennard-Jones potential,  $U=4\epsilon((\sigma/x)^{12}-(\sigma/x)^6)$ , where  $\sigma$ =collision radius=3.6 Å, and  $\epsilon$ =reduced potential from Ref. 15=82.3 K. The interactions between adsorbate molecules are neglected. Cylindrical symmetry is taken for the

evaluation of the integrated interaction of a Xe atom with the carbon atoms in the SWNT.

<sup>41</sup>B. K. Peterson, K. E. Gubbins, G. S. Heffelfinger, U. Marini Bettolo Marconi, and F. van Swol, *J. Chem. Phys.* **88**, 6487 (1988).

<sup>42</sup>W. Teizer, R. B. Hallock, E. Dujardin, and T. W. Ebbesen, *Phys. Rev. Lett.* **82**, 5305 (1999).

<sup>43</sup>J. P. Miller *et al.*, *J. Chem. Phys.* **87**, 6725 (1987).